Monthly Notices
of the
ROYAL ASTRONOMICAL SOCIETY

MNRAS **475,** 4467–4475 (2018)
Advance Access publication 2017 November 3

doi:10.1093/mnras/stx2778

NGTS-1b: a hot Jupiter transiting an M-dwarf

Daniel Bayliss,[1★] Edward Gillen,[2★] Philipp Eigmüller,[3] James McCormac,[4,5] Richard D. Alexander,[6] David J. Armstrong,[4,5] Rachel S. Booth,[7] François Bouchy,[1] Matthew R. Burleigh,[6] Juan Cabrera,[3] Sarah L. Casewell,[6] Alexander Chaushev,[6] Bruno Chazelas,[1] Szilard Csizmadia,[3] Anders Erikson,[3] Francesca Faedi,[4] Emma Foxell,[4] Boris T. Gänsicke,[4,5] Michael R. Goad,[6] Andrew Grange,[6] Maximilian N. Günther,[2] Simon T. Hodgkin,[8] James Jackman,[4] James S. Jenkins,[9,10] Gregory Lambert,[2] Tom Louden,[4,5] Lionel Metrailler,[1] Maximiliano Moyano,[11] Don Pollacco,[4,5] Katja Poppenhaeger,[7] Didier Queloz,[2] Roberto Raddi,[4] Heike Rauer,[3,12] Liam Raynard,[6] Alexis M. S. Smith,[3] Maritza Soto,[9] Andrew P. G. Thompson,[7] Ruth Titz-Weider,[3] Stéphane Udry,[1] Simon. R. Walker,[4] Christopher A. Watson,[7] Richard G. West[4,5] and Peter J. Wheatley[4,5]

Affiliations are listed at the end of the paper

Accepted 2017 October 23. Received 2017 October 19; in original form 2017 September 13

ABSTRACT

We present the discovery of NGTS-1b, a hot Jupiter transiting an early M-dwarf host ($T_{\rm eff,*} = 3916^{+71}_{-63}$ K) in a $P = 2.647$ d orbit discovered as part of the Next Generation Transit Survey (NGTS). The planet has a mass of $0.812^{+0.066}_{-0.075}\,M_{\rm J}$, making it the most massive planet ever discovered transiting an M-dwarf. The radius of the planet is $1.33^{+0.61}_{-0.33}\,R_{\rm J}$. Since the transit is grazing, we determine this radius by modelling the data and placing a prior on the density from the population of known gas giant planets. NGTS-1b is the third transiting giant planet found around an M-dwarf, reinforcing the notion that close-in gas giants can form and migrate similar to the known population of hot Jupiters around solar-type stars. The host star shows no signs of activity, and the kinematics hint at the star being from the thick disc population. With a deep (2.5 per cent) transit around a $K = 11.9$ host, NGTS-1b will be a strong candidate to probe giant planet composition around M-dwarfs via *James Webb Space Telescope* transmission spectroscopy.

Key words: techniques: photometric – techniques: radial velocities – stars: individual: NGTS-1 – planetary systems.

1 INTRODUCTION

M-dwarf stars as planetary hosts are of high interest. Two important recent discoveries in the field of exoplanets relate to planets orbiting M-dwarfs: Proxima Centauri (Anglada-Escudé et al. 2016) and Trappist-1 (Gillon et al. 2017). The interest primarily derives from the fact that the radius ratio ($R_{\rm P}/R_{\rm star}$) and mass ratio ($M_{\rm P}/M_{\rm star}$) for such systems are much higher than equivalent systems with solar-type hosts, thus they can be easier to detect via transits and radial velocities. The low intrinsic luminosity of M-dwarfs also means that the habitable zone is very close to the host star and therefore it is much easier to detect potential habitable planets around these stars, compared to their more massive counterparts. Finally, M-dwarfs are the most populous stars in the Galaxy (∼75 per cent; Henry et al. 2006), and hence understanding planet formation and planet frequency around these low-mass stars greatly enhances our knowledge of the full population of planets in the Galaxy.

However, observationally M-dwarfs present some significant drawbacks when searching for exoplanets. First, the intrinsically low luminosity of M-dwarfs means that on average they have much fainter apparent magnitudes than solar-type stars, making it hard to obtain high-precision photometry or high-precision radial velocity measurements. Secondly, the spectra of M-dwarfs are dominated by molecular lines which do not allow the same precision radial velocity measurements as are afforded by the unblended, sharp metal

★ E-mail: daniel.bayliss@unige.ch, d.bayliss@warwick.ac.uk (DB); ecg41@cam.ac.uk (EG)

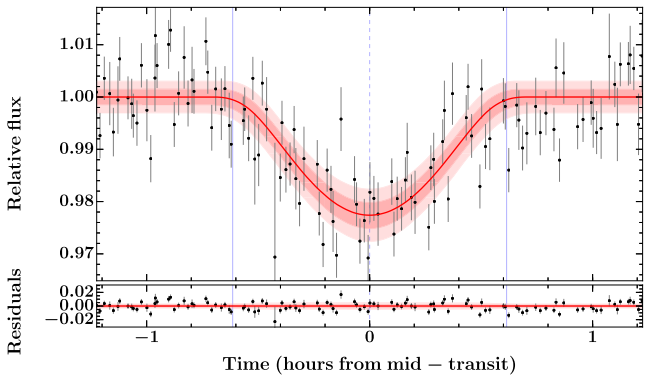

Figure 1. The NGTS light curve of NGTS-1 phase-folded at the best-fitting period of 2.647 298 ± 0.000 020 d and zoomed to show the transit event. Black circles show the photometric data points binned to 10-minutes with associated photon error. The red line and pink shaded regions show the median and the 1- and 2-sigma uncertainties, respectively, of the posterior model based on the global modelling set out in Section 3.2. Solid blue vertical lines indicate the start of ingress (T_1) and end of egress (T_4). Dashed blue vertical line represents the transit centre (T_c). Residuals to the global model are shown below the light curve.

lines that can be found in solar-type spectra. Finally, the low effective temperatures of M-dwarfs mean they have a peak flux well outside the optical wavelength range where most photometry and spectroscopy is targeted.

Despite these difficulties there has been progress in identifying exoplanets orbiting M-dwarfs using dedicated facilities. Notably, the Earth-sized GJ1132-b (Berta-Thompson et al. 2015) and super-Earth GJ1214-b (Charbonneau et al. 2009), detected with the MEarth ground-based transit survey (Nutzman & Charbonneau 2008), have been popular targets for atmospheric characterization owing to the small radii and close proximity to Earth of their M-dwarf hosts. A large radial velocity programme to monitor M-dwarfs, carried out by the HARPS consortium (Mayor et al. 2003; Bonfils et al. 2005), has produced more than 10 confirmed exoplanets and recently two planets orbiting GJ 273 – potentially making this the closest known system with planets in the habitable zone after Proxima Centauri (Berdiñas 2016; Astudillo-Defru et al. 2017). The Kepler and K2 missions, while not designed to specifically target M-dwarfs, have discovered transiting planets around M-dwarfs in their field of view: Kepler-138b (Rowe et al. 2014); K2-33b (David et al. 2016). In addition to these programmes the wide-field Next Generation Transit Survey (NGTS) survey is underway. NGTS is optimized to detect transits around K and early M-dwarfs and is at the limit of photometric precision possible for ground-based observations (Chazelas et al. 2012; Wheatley et al. 2013; McCormac et al. 2017; Wheatley 2017).

Small planets (0.5–4 $R_\oplus$) appear to be common around M-dwarfs (Dressing & Charbonneau 2013), and gas giants are considerably rare. Meyer et al. (2017) give the frequency of planets with masses 1–10 M_J as 0.07 planets per M-dwarf. To date, only two gas giant planets have been discovered transiting M-dwarfs – namely Kepler-45b ($M_p = 0.505\,M_J$, $R_p = 0.96\,R_J$; Johnson et al. 2012) and HATS-6b ($M_p = 0.32\,M_J$, $R_p = 1.00\,R_J$; Hartman et al. 2015). WASP-80b ($M_p = 0.55\,M_J$, $R_p = 0.95\,R_J$; Triaud et al. 2013) also transits a low-mass host star very similar to these early M-dwarfs, and is close in its physical properties to Kepler-45b. However, hot Jupiters are rare around solar-type stars also – from Kepler statistics the frequency of hot-Jupiter systems around solar-type stars is 0.43 ± 0.05 for $P < 10$ d (Fressin et al. 2013). Coupled to this, transit surveys have not monitored large numbers of M-dwarfs compared with the solar-type population. Thus, a larger population of M-dwarfs needs to be monitored in order to ascertain if the frequency of hot Jupiters around M-dwarfs significantly departs from the solar-type frequency.

In this paper we report the discovery of NGTS-1b, the third gas giant found to transit an M-dwarf. In Section 2 we detail the observations that led to the discovery of this planet, including the NGTS survey photometry, high-precision follow-up photometry, and high-resolution spectroscopy. In Section 3 we analyse the observational data in conjunction with archival photometric data to precisely determine the physical characteristics of NGTS-1b. Finally, in Section 4 we discuss the results including the significance of this discovery in terms of planet formation scenarios around low-mass stars and the prospects for characterization via *James Webb Space Telescope* (*JWST*).

2 OBSERVATIONS

The discovery of NGTS-1b was made using the NGTS telescopes in conjunction with high-precision photometric follow-up from Eulercam and high-precision spectroscopy from HARPS. We detail all of these observations in this section.

2.1 NGTS photometry

NGTS is a fully automated array of twelve 20-cm aperture Newtonian telescopes situated at the ESO Paranal Observatory in Chile. Each telescope is coupled to an Andor Ikon-L Camera featuring a 2K × 2K e2V deep-depleted CCD with 13.5 μm pixels, which corresponds to an on-sky size of 4.97 arcsec. Telescopes are operated from independent Optical Mechanics, Inc. (OMI) mounts, allowing for excellent tracking and freedom in scheduling observations.

NGTS-1 was observed on a single NGTS telescope over a photometric campaign conducted between 2016 August 10 and 2016 December 7. In total we obtained 118 498 × 10 s exposures in the NGTS bandpass (550–927 nm) over ∼100 usable nights. Raw data were reduced to calibrated fit frames via the NGTS reduction pipeline fully described in Wheatley (2017). Photometry was extracted via aperture photometry using the NGTS photometric pipeline, which is a customized implementation of the CASUTOOLS[1] photometry package. To account for systematic effects in the data, an implementation of the SysRem algorithm (Tamuz, Mazeh & Zucker 2005) was applied to the data. Again full details can be found in Wheatley (2017).

Light curves were searched for transit-like signals using ORION, an implementation of the box-fitting least squares (BLS) algorithm (Kovács, Zucker & Mazeh 2002). We identified a strong BLS signal for NGTS-1 at a period of 2.647 298 ± 0.000 020 d.

We set out the transit feature identified in the NGTS light curve, phase-folded to this period, in Fig. 1, and provide the full light-curve data set in Table 1.

Our previous yield simulations have evaluated the risk of false positives mimicking a planetary transit such as NGTS-1 (Günther et al. 2017a). In order to verify that this transit signal is consistent with a transiting planet, we applied a series of vetting tests to the NGTS data.

First, we checked the light curve for evidence of a secondary eclipse near phase 0.5. Such a detection, at our photometric precision, would indicate an eclipsing stellar companion rather than

[1] http://casu.ast.cam.ac.uk/surveys-projects/software-release

Table 1. NGTS photometry for NGTS-1. The full table is available in a machine-readable format from the online journal. A portion is shown here for guidance.

Time (HJD-2450000)	Flux (normalized)	Flux error
7610.84860	0.9633	0.0315
7610.84875	1.0530	0.0317
7610.84890	1.0636	0.0317
7610.84905	1.0216	0.0317
7610.84920	0.9808	0.0317
7610.84935	1.0042	0.0317
7610.84949	1.0401	0.0317
7610.84964	1.0316	0.0316
7610.84979	0.9792	0.0316
7610.84994	1.0067	0.0317
...	...	...

Table 2. z -band Eulercam photometry for NGTS-1. The full table is available in a machine-readable format from the online journal. A portion is shown here for guidance.

Time (HJD-2450000)	Flux (normalized)	Flux error
7810.59349558	1.000691	0.001658
7810.59571697	1.001244	0.001659
7810.59793916	1.000230	0.001657
7810.60016845	0.999125	0.001655
7810.60247724	1.001336	0.001659
7810.60469833	1.000415	0.001657
7810.60691832	1.004940	0.001665
7810.60921191	0.999217	0.001655
7810.61142560	1.002259	0.001660
7810.61364589	1.000875	0.001658
...	...	...

a transiting planet companion. However no secondary eclipse is detected.

Secondly, we checked the odd/even transit depth differences to help rule out the possibility that we have detected half the true period, and have phase-folded primary and secondary eclipses together. We see no odd/even depth difference to the precision of our photometry.

Thirdly, we check for out-of-transit ellipsoidal variation that is present in many short-period binary stars. Again, no such variability is seen to the precision of our photometry.

Finally, we check for a shift in the photometric centre-of-flux during transit events as fully described in Günther et al. (2017b). This test is able to detect blended eclipsing binaries at separations well below the size of individual NGTS pixels – i.e. to the level of ∼1 arcsec. We find no centroiding variation during the transit events of NGTS-1.

Using existing photometric and proper motion survey data (see Table 4), we identified that NGTS-1 is a low-temperature star, and in combination with the stellar populations from the Besançon Galaxy model (Robin et al. 2003) we concluded that NGTS-1 is most likely an M-dwarf rather than an M-giant. This means that the deep (2.5 per cent) and V-shaped transit is still consistent with a transiting body being of planetary radius, and therefore we passed this candidate on for further photometric and spectroscopic follow-up, as detailed in Sections 2.2 and 2.3.

2.2 Eulercam photometry

In order to refine the ephemeris, increase the precision of the light-curve component of the global modelling (see Section 3.2), and check for any evidence of a blend via a colour-dependent depth difference, we obtained a high-precision light curve for NGTS-1 using Eulercam on the 1.2-m Euler Telescope at La Silla Observatory. Observations were taken on the night of 2017 February 26 between 2:14 and 5:08 UT in the z band with the telescope slightly defocused (0.5 mm) to broaden the point-spread function. In total 50 exposures were obtained, each with an exposure time of 180 s. After the images were reduced via standard bias and flat-field correction, we performed aperture photometry on NGTS-1 and a set of 10 reference stars using a photometric pipeline utilizing Source Extractor (Bertin & Arnouts 1996). A full transit event was observed, and the photometric data are presented in Table 2, while the data are plotted with a best-fitting transit model in Fig. 2. These data are used in the global modelling for the NGTS-1b system detailed in Section 3.2.

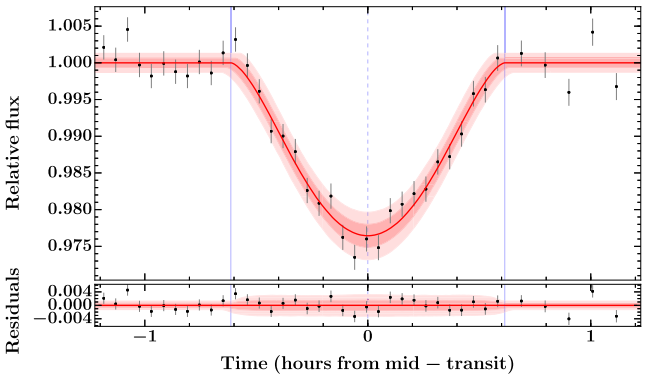

Figure 2. The z-band Eulercam light curve for NGTS-1 on the UT night of 2017 February 26 from La Silla Observatory, Chile. Black data points are the individual 180 s exposures. All other symbols as for Fig. 1.

2.3 Spectroscopy

We obtained multi-epoch spectroscopy for NGTS-1 with the HARPS spectrograph (Mayor et al. 2003) on the ESO 3.6 m telescope at La Silla Observatory, Chile, between 2017 January 27 and 2017 February 7. Due to the faint optical magnitude of NGTS-1 ($V = 15.52 \pm 0.08$), we used the HARPS in the high-efficiency fibre link (EGGS) mode, which utilizes a slightly larger fibre (1.4 arcsec compared with the 1.0 arcsec in nominal mode). This gives a higher signal-to-noise ratio spectrum, albeit with a slightly lower resolution ($R = 85\,000$ compared with $R = 110\,000$). To further increase the signal-to-noise ratio we took long exposures (1-h) for each epoch.

Using the standard HARPS data reduction pipeline, radial velocities were calculated for each epoch via cross-correlation with the M2 binary mask. These radial velocities are listed, along with their associated error, full width at half maximum (FWHM), contrast and bisector slope, in Table 3. The radial velocities show a variation in-phase with the photometric period and phase. The semi-amplitude is large ($K = 166 \pm 11\,\mathrm{m\,s^{-1}}$), indicating a Jupiter-mass planet. We plot the phase-wrapped radial velocities in Fig. 3. Again, these data are used in the global modelling for the NGTS-1b system detailed in Section 3.2.

We also wavelength shift and combine all seven spectra to create a single, high signal-to-noise ratio spectrum from HARPS. This spectrum is used to characterize the stellar properties of NGTS-1 (see Section 3.1).

Table 3. Radial velocities for NGTS-1.

HJD (−2450000)	RV (km s^{-1})	RV err (km s^{-1})	FWHM (km s^{-1})	Contrast	BIS (km s^{-1})
7780.712430	97.310	0.023	3.783	10.7	−0.080
7784.657148	97.032	0.013	3.718	11.3	−0.011
7785.598834	97.218	0.011	3.730	11.3	−0.011
7786.618897	97.268	0.013	3.671	11.1	−0.044
7789.645749	97.121	0.015	3.737	11.1	−0.035
7790.641250	97.106	0.017	3.735	10.7	−0.012
7791.655373	97.336	0.015	3.693	10.5	−0.006

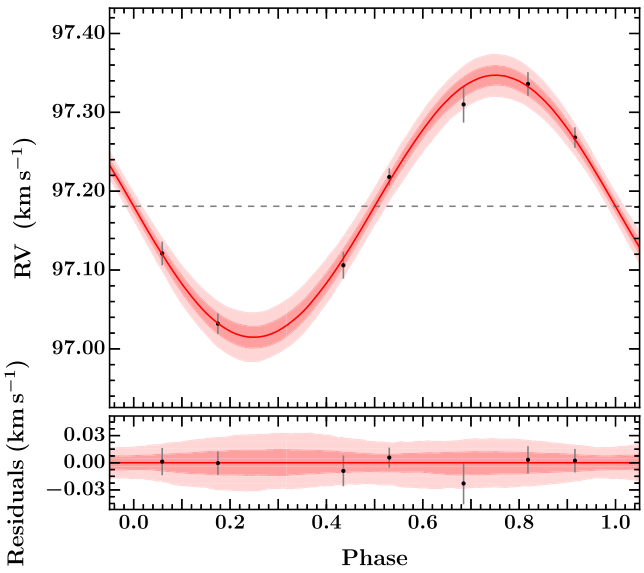

Figure 3. Phase-wrapped radial velocity measurements for NGTS-1 from the HARPS spectrograph on the ESO 3.6 m at La Silla Observatory, Chile. The red line and pink shaded regions show the median and the 1- and 2-sigma uncertainties, respectively, of the posterior model based on the global modelling set out in Section 3.2. The horizontal dashed line shows the systemic radial velocity of NGTS-1. The residuals to the global model are shown below the radial velocity data.

3 ANALYSIS

The observations made in Section 2 are combined with archival data from various photometric surveys in order to fully characterize the NGTS-1b system. In this section we detail that analysis, in addition to analysing the data for stellar activity, rotation and background contamination.

3.1 Stellar properties

One of the difficulties with characterizing M-dwarfs is that in the optical they are faint and have spectra dominated by strong molecular bands (Lépine et al. 2013). Metallicity is especially difficult to determine, with the best methods requiring *K*-band spectra to measure the Ca I and Na I lines from 2.2 to 2.3 μm (Rojas-Ayala et al. 2010). This impacts the stellar parameters since the stellar radius for M-dwarfs is highly metallicity dependent.

Nevertheless, we are able to use the combined HARPS spectrum (see Section 2.3) to spectral-type NGTS-1. We compared the combined HARPS spectrum using M-dwarf spectral templates derived from the Sloan Digital Sky Survey (Rebassa-Mansergas et al. 2007). The HARPS spectrum is not globally flux-calibrated, and we therefore fitted the M-dwarf templates over a 100 Å wide band of the

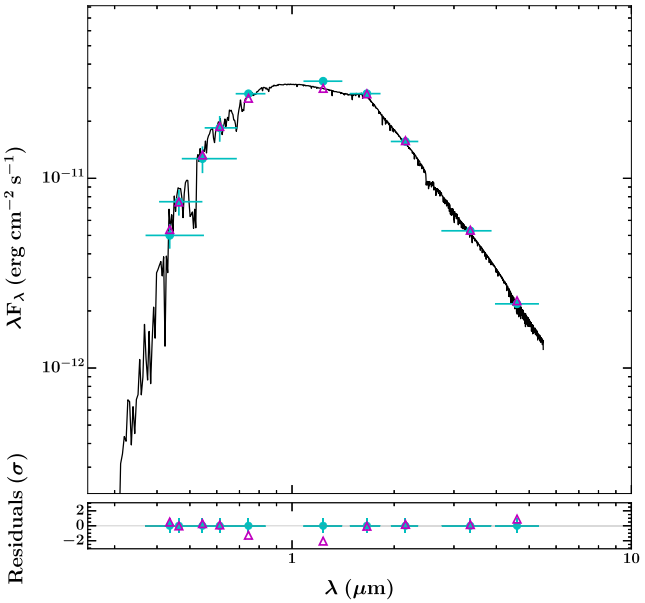

Figure 4. The fitted SED (black line) for NGTS-1 based on the photometric data (cyan points) presented in Table 4. The magenta triangles show the model flux at the wavelengths of the photometric data.

HARPS spectrum, recording the value of the local χ^2. This band was then sliced across the full spectral range, and a global χ^2 was computed from the sum of all the local values. The spectral type determined from this procedure is M0.5 ± 0.5, any later types are clearly excluded by the relative strengths of the molecular absorption bands, and by the width of the Na I 5890/96 Å lines. Although metallicity cannot be well determined, we see no evidence of the star being extremely metal rich or poor in comparison to M-dwarf templates (Savcheva, West & Bochanski 2014), and therefore we adopt a metallicity of [M/H] = 0 for our analysis. From the HARPS spectrum we can also place an upper limit on the *v*sin*i* of NGTS-1 at 1.0 km s^{-1}, consistent with the possible rotational period derived from the photometry and discussed in Section 3.3.

Given the indication from the combined HARPS spectrum that the host was an early M-dwarf, we utilize the recent empirical relations that are based on extensive studies of nearby M-dwarfs. In particular, we use the relations of Mann et al. (2015) (hereafter M15) and Benedict et al. (2016) (hereafter B16), along with modelling the stellar SED, to estimate mass, radius and $T_{\rm eff}$ values for NGTS-1. We took three main steps:

(i) We estimated $T_{\rm eff}$, radius and mass using M15. $T_{\rm eff}$ was estimated from the system's broad-band colours, which gave $T_{\rm eff} = 3867 \pm 107$ K. The radius was then estimated from this $T_{\rm eff}$ value, which gave $R_{\rm s} = 0.573 \pm 0.077\,{\rm R}_\odot$ (note this is not a tight relation given we do not know the metallicity.). The radius was then used to determine the absolute $K_{\rm s}$ band magnitude ($M_{K_{\rm s}}$), which in turn gave an expected mass of $M_{\rm s} = 0.598 \pm 0.011\,{\rm M}_\odot$. This step is not particularly intuitive, but it becomes possible because of the implicit $T_{\rm eff}$ prediction underlying the radius estimation and the fact that the error ellipses in $T_{\rm eff}$–radius space and radius–$M_{K_{\rm s}}$ space are orthogonal. We use this mass estimate only to check our final value.

(ii) We modelled the spectral energy distribution (SED) of NGTS-1 (Fig. 4) using the method described in Gillen et al. (2017). Briefly, we convolved the BT-SETTL and PHOENIX v2 model atmospheres (Allard, Homeier & Freytag 2011) with the available bandpasses (see Table 4) and interpolated in $T_{\rm eff}$–log g space

Table 4. Stellar properties for NGTS-1.

Property	Value	Source
Astrometric properties		
R.A.	$05^{h}30^{m}51\overset{s}{.}45$	2MASS
Dec.	$-36°37'50\overset{''}{.}83$	2MASS
2MASS I.D.	J05305145 − 3637508	2MASS
$\mu_{R.A.}$ (mas y^{-1})	-32.9 ± 2.0	UCAC4
$\mu_{Dec.}$ (mas y^{-1})	-39.6 ± 1.8	UCAC4
Photometric properties		
V (mag)	15.524 ± 0.083	APASS
B (mag)	16.912 ± 0.077	APASS
g (mag)	16.288 ± 0.000	APASS
r (mag)	14.999 ± 0.006	APASS
i (mag)	14.328 ± 0.022	APASS
G_{Gaia}(mag)	14.702 ± 0.001	*Gaia*
NGTS (mag)	14.320 ± 0.02	This work
J (mag)	12.702 ± 0.024	2MASS
H (mag)	12.058 ± 0.022	2MASS
K (mag)	11.936 ± 0.027	2MASS
$W1$ (mag)	11.800 ± 0.023	WISE
$W2$ (mag)	11.779 ± 0.022	WISE
Derived properties		
T_{eff} (K)	3916^{+71}_{-63}	SED fitting
[M/H]	0	HARPS Spectrum
$v\sin i$ (km s^{-1})	<1.0	HARPS Spectrum
γ_{RV} (km s^{-1})	97.1808 ± 0.0070	HARPS Spectrum
log g	4.71 ± 0.23	ER
M_s(M$_\odot$)	$0.617^{+0.023}_{-0.062}$	ER
R_s(R$_\odot$)	0.573 ± 0.077	ER
ρ (g cm^{-3})	$4.4^{+2.4}_{-1.4}$	ER
Distance (pc)	224^{+37}_{-44}	SED fitting

2MASS (Skrutskie et al. 2006); UCAC4 (Zacharias et al. 2013); APASS (Henden & Munari 2014); WISE (Wright et al. 2010); *Gaia* (Gaia Collaboration et al. 2016).
ER = empirical relations using B16 and Mann et al. (2015).

(fixing [M/H] = 0) within a Markov chain Monte Carlo (MCMC) and placed the following priors: a uniform (but not uninformative) prior on the radius: $0.4\,R_\odot \leq R_s \leq 0.7\,R_\odot$, which brackets plausible radius estimates given the expected T_{eff} range; a Gaussian prior on $\log g$: $\log g = 4.7 \pm 0.2$, which is estimated from the predictions of the PARSEC v1.2 stellar evolution models given our T_{eff}, M and R estimates (with the uncertainty further inflated); a Gaussian prior on A_V: $A_V = 0.0 \pm 0.1$ (positive values allowed only) following initial tests implying a low-to-negligible reddening; uninformative priors on the T_{eff} and distance; and an uninformative prior on the uncertainties, which are fit for within the MCMC. Combining the results from the BT-SETTL and PHOENIX models gives $T_{eff} = 3916^{+71}_{-63}$ K and distance $d = 224^{+37}_{-44}$ pc.

(iii) We then used our SED modelling results and the M_{K_s}–mass relation of B16 to determine $M_s = 0.617^{+0.023}_{-0.062}\,M_\odot$. We note that this is in agreement with the M15 value.

We adopt, as our final stellar parameters, the T_{eff} and distance estimates from our SED modelling, the radius estimate from M15 and the mass estimate from B16; these are reported in Table 4.

3.2 Global modelling

Using the photometric and radial velocity data set out in Section 2, in addition to the stellar parameters set out in Section 3.1, we globally model the system in order to determine the stellar and planetary parameters for the NGTS-1b system. We use the GP-EBOP transiting planet and eclipsing binary model. GP-EBOP is fully described in Gillen et al. (2017), where it is applied to eclipsing binaries and a transiting brown dwarf, and we further note its tested ability to model transiting planets [see e.g. Pepper et al. (2017)]. In GP-EBOP, the full light curve is modelled as a Gaussian process, whose mean function is a transit model. The radial velocity data are modelled simultaneously with the available photometry and incorporate a jitter term to allow for stellar activity variations and instrumental systematics in the data. GP-EBOP explores the posterior parameter space using an affine-invariant MCMC. We use priors on stellar density and limb darkening parameters following Gillen et al. (2017).

One difficulty in modelling this system is that the transit is grazing, which is relatively likely given the radius ratio between the planet and the star ($0.239^{+0.100}_{-0.054}$). Such a configuration results in a strong degeneracy between the impact parameter (b) and the planetary radius (R_p). To help break this degeneracy we construct a prior on the radius of the planet based on the existing population of hot Jupiters. To a first approximation the two measurable quantities that influence the radius of hot Jupiters are mass (Hatzes & Rauer 2015) and incident flux (Demory & Seager 2011). Using the NASA Exoplanet Archive[2] (Akeson et al. 2013), we take the population of transiting hot Jupiters ($M_p > 0.2\,M_J$, $P < 50$ d) with incident fluxes in a similar regime to NGTS-1b ($<2 \times 10^8$ erg s^{-1} cm^{-2}). This cut on incident flux is important as it excludes highly inflated hot Jupiters at high incident fluxes (Demory & Seager 2011). The resulting population shows a lognormal distribution of densities, with ln(density) having a mean at -0.29 and a standard deviation of 0.89. We apply this lognormal density distribution as a prior on the density of NGTS-1b during the global modelling. We present the fitted and derived parameters using this prior as our final parameters and list them in Table 5. We also present in Table 5 the parameters without any prior on the planet density.

To illustrate the impact of this prior, Fig. 5 shows the posterior distributions for five key model parameters with and without the planet density prior. Most importantly we see the radius ratio (R_p/R_s) moves from an almost unconstrained posterior distributions to a more physically realistic distribution. We caution that this approach means that the radius we measure for this planet is not as robust as for most transiting gas giants in the literature, and simply represents our best estimate based on all available data for this system and the population gas giant planets in general.

Using these parameters from the GP-EBOP global modelling and the stellar properties as derived in Section 3.1, we derive the planet parameters for NGTS-1b. These planet parameters are set out in Table 6, and show that NGTS-1b is a Jupiter mass ($0.812^{+0.066}_{-0.075}\,M_J$) planet with a radius of $1.33^{+0.61}_{-0.33}\,R_J$.

3.3 Stellar activity and rotation

The analysis of the Hα line in the combined HARPS spectrum does not show any sign of emission that we would associate with activity, and there is no flaring detected in the NGTS photometry. The star is not coincident with any catalogued X-ray source, and there is no X-ray detection in the XMM-Slew survey (Saxton et al. 2008). The XMM-Slew survey data provide a model-dependent upper limit of 5.7×10^{-13} erg s^{-1} cm^{-2} in the 0.2–2 keV band, and across the 0.2–12 keV band the upper limit is 1.4×10^{-12} erg s^{-1} cm^{-2}. This is not

[2] exoplanetarchive.ipac.caltech.edu

Table 5. Fitted and derived parameters of the models applied to ecc + ρ_* prior and ecc + ρ_* and ρ_{pl} priors.

Parameter	Symbol	Unit	Value	
			ecc + ρ_* prior	ecc + ρ_* & ρ_{pl} priors
		Transit parameters		
Sum of radii	$(R_s + R_p)/a$		0.139 ± 0.034	$0.1021^{+0.0108}_{-0.0087}$
Radius ratio	R_p/R_s		$0.76^{+0.68}_{-0.47}$	$0.239^{+0.100}_{-0.054}$
Orbital inclination	i	°	82.8 ± 2.3	$85.27^{+0.61}_{-0.73}$
Orbital period	P	d	2.647297 ± 0.000021	2.647298 ± 0.000020
Time of transit centre	T_{centre}	BJD	$2457720.65939 \pm 0.00067$	$2457720.65940 \pm 0.00062$
	$\sqrt{e}\cos\omega$		0.01 ± 0.11	-0.001 ± 0.098
	$\sqrt{e}\sin\omega$		0.05 ± 0.12	0.02 ± 0.12
Linear LDC	u_{NGTS}		0.40 ± 0.14	0.46 ± 0.13
Non-linear LDC	u'_{NGTS}		0.14 ± 0.23	0.12 ± 0.2
Linear LDC	u_{Euler}		0.30 ± 0.11	0.322 ± 0.083
Non-linear LDC	u'_{Euler}		0.21 ± 0.24	0.21 ± 0.18
		Out-of-transit variability parameters		
Amplitude	A_{NGTS}	per cent	$0.00228^{+0.00033}_{-0.00027}$	$0.00228^{+0.00035}_{-0.00028}$
Time-scale	l_{NGTS}	d	$2.76^{+0.29}_{-0.46}$	$2.76^{+0.29}_{-0.45}$
White noise term	σ_{NGTS}		1.180 ± 0.016	1.181 ± 0.017
Amplitude	A_{Euler}	per cent	$0.035^{+0.056}_{-0.025}$	$0.065^{+0.179}_{-0.050}$
Time-scale	l_{Euler}	d	$2.32^{+0.61}_{-0.83}$	$2.48^{+0.50}_{-0.82}$
White noise term	σ_{Euler}		1.16 ± 0.13	1.17 ± 0.13
		Radial velocity parameters		
Systemic velocity	V_{sys}	$km\,s^{-1}$	$97.1801^{+0.0071}_{-0.0078}$	97.1809 ± 0.0070
Primary RV semi-amplitude	K_{pri}	$km\,s^{-1}$	0.166 ± 0.012	0.166 ± 0.011
HARPS White noise term	σ_{HARPS}	$km\,s^{-1}$	$0.0080^{+0.0116}_{-0.0057}$	$0.0071^{+0.0101}_{-0.0049}$

LDC = limb darkening coefficient.

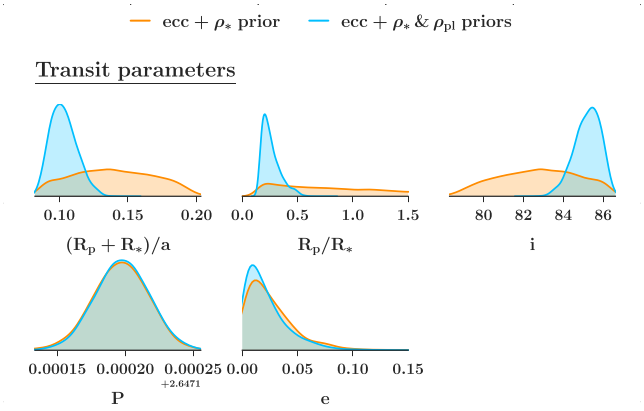

Figure 5. The posterior distributions for five key parameters from the GP-EBOP global modelling with a prior on the stellar density, free-eccentricity and with/without (blue/orange) the adoption of the planet density prior.

surprising as M-dwarfs of this effective temperature are expected to have flux levels below this upper limit (Stelzer et al. 2013).

M-dwarfs often have a larger fraction of spot coverage on their surface in comparison to FGK stars, and such spots may be revealed in photometric data as long-term variability at the stellar rotation period. To investigate this for NGTS-1 we ran the CLEAN algorithm (Roberts, Lehar & Dreher 1987) to identify periods and a Lomb–Scargle analysis (Lomb 1976) to estimate their significance using the NGTS photometric data. The result is set out in Fig. 6. No significant signal was found. The broad peak at a period of approximately 43 d corresponds to a signal with an amplitude of ≈1.5 mmag, which is at the level of expected systematic noise. However, such a rotation period would be consistent with rotation rates for low-activity M-dwarfs (McQuillan, Aigrain & Mazeh 2013), and is similar to the other M-dwarf gas planet host, HATS-6, which has a probable rotation period of 35.1 d (Hartman et al. 2015).

3.4 Archival images

Due to the relatively high proper motion of NGTS-1 (-32.9 ± 2.0 mas y^{-1}, -39.6 ± 1.8 mas y^{-1}), we are able to study archival images of NGTS-1 to help rule out blended background stars currently within the point-spread function of NGTS-1. The earliest image available is a photographic plate taken in 1976 December 26 as part of the SERC-J Survey on the UK Schmidt 1.2 m telescope at Siding Spring Observatory, Australia. The plate has been digitized as part of the STScI Digitized Sky Survey. From this image we identify NGTS-1 at 05:30:51.543, −36:37:50.49. Subsequent Digitized Sky Survey images are from 1985, 1992 and 1995. 2MASS imaged NGTS-1 in 1999. Our own imaging is from 2016. From these images we confirm the high proper motion, totalling 2.7 arcsec over 40 years. This is consistent with the proper motion as reported in UCAC4 (see Table 4). The archival imaging allows us to rule out any background star at a significant flux level within the current NGTS point-spread function.

3.5 Kinematics

Using the proper motion (R.A.: -32.9 ± 2.0 mas y^{-1}, Dec.: -39.6 ± 1.8 mas y^{-1}), the absolute radial velocity (97.1808 ± 0.0070 km s^{-1}) and the estimated distance of 224^{+37}_{-44} pc, we calculate the (U_{LSR}, V_{LSR}, W_{LSR}) galactic motion for NGTS-1 to be (11.3 ± 8.3, -57.2 ± 1.6, -79.7 ± 7.6) km s^{-1}. This

Table 6. Planetary properties for NGTS-1b.

Property	Value
P (d)	$2.647\,298 \pm 0.000\,020$
T_C (HJD)	$2457720.6593965 \pm 0.00062$
T_{14} (h)	1.23 ± 0.04
a/R_*	12.2 ± 0.7
b	$0.9948^{+0.13}_{-0.088}$
K (m s^{-1})	166 ± 11
e	$0.016^{+0.023}_{-0.012}$
$M_p(M_J)$	$0.812^{+0.066}_{-0.075}$
$R_p(R_J)$	$1.33^{+0.61}_{-0.33}$
ρ_p (g cm^{-3})	$0.42^{+0.59}_{-0.28}$
a (au)	$0.0326^{+0.0047}_{-0.0045}$
T_{eq} (K)	790 ± 20
Flux (erg s^{-1} cm^{-2})	$(8.89 \pm 0.70) \times 10^7$

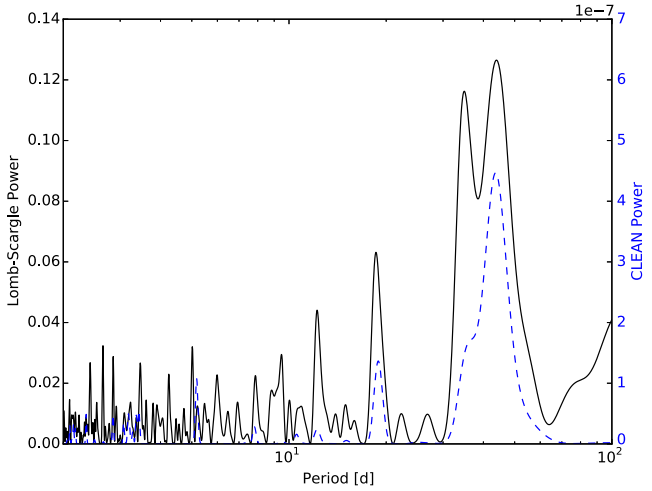

Figure 6. The Lombe–Scargle periodogram (black, continuous line) and the CLEAN periodogram (blue, dashed line) for NGTS-1 from the NGTS photometric data. The peak at 43 d may be due to spot rotation.

suggests that NGTS-1 is a member of the thick disc population, and may therefore be a very old system. The major uncertainty in obtaining the galactic motion is the uncertainty in the distance to NGTS-1. It will be interesting to confirm the motion after the second *Gaia* data release (Gaia Collaboration et al. 2016), which will provide a much more precise distance for NGTS-1.

4 DISCUSSION

NGTS-1b is a Jupiter-mass planet orbiting an M0-dwarf star in a $2.647\,298 \pm 0.000\,020$ d period. As such, it is just the third transiting gas giant to be discovered around an M-dwarf, and with $M_p = 0.812^{+0.066}_{-0.075}\,M_J$ it is easily the most massive planet known transiting an M-dwarf. The two previously discovered examples are Kepler-45b ($M_p = 0.505 M_J$, $R_p = 0.96 R_J$; Johnson et al. 2012) and HATS-6b ($M_p = 0.32 M_J$, $R_p = 1.00 R_J$; Hartman et al. 2015). Due to the grazing nature of the transit, the radius of NGTS-1b is not well constrained and is strongly influenced by the density prior we use. Our hope is that 2-min cadence data from the NASA *Transiting Exoplanet Survey Satellite* (*TESS*) mission (Ricker et al. 2014) will allow us to improve this estimate and model the system without the need for a prior on the planet density.

4.1 Giant planet formation around M-dwarfs

Planet formation theory suggests that giant planets should be rarer around M-dwarfs than around FGK stars (Kennedy & Kenyon 2008). Dynamical time-scales around lower-mass stars are longer, slowing the process(es) of planet formation (e.g. Laughlin, Bodenheimer & Adams 2004), and the mass budget is also lower (as protoplanetary disc masses decrease approximately linearly with stellar mass; Andrews et al. 2013). Thus, determining the frequency of giant planets around M-dwarfs should yield important new insights into the planet formation process.

It has long been known that for solar-type host stars the incidence of giant planets increases very sharply with increasing host star metallicity (Fischer & Valenti 2005), and very few giant planets have been detected around stars with significantly sub-solar metallicity. However, the same correlation is not seen for Neptunes or super-Earths, whose incidence appears largely independent of metallicity (Sousa et al. 2008; Buchhave & Latham 2015; Jenkins et al. 2017). By robustly determining the metallicity of NGTS-1 and systems like this we will be able to probe if the correlation between metallicity and giant planet frequency remains true for low-mass stars.

Probing the frequency of gas giants, and in particular, hot Jupiters orbiting M-dwarfs, is difficult. The intrinsic low luminosity of M-dwarfs makes them hard to monitor for radial velocity surveys. The largest M-dwarf radial velocity survey, by Bonfils et al. (2013), was able to put an upper limit of ≈1 per cent for $P < 10$ d and masses of $0.1 < m \sin i < 1.0\,M_J$. However, this result does not constrain M-dwarfs to have a lower frequency of hot Jupiters than FGK stars, which is robustly determined from the Kepler mission to be 0.43 ± 0.05 per cent for $P < 10$ d and $0.55 < R_p < 2$ (Fressin et al. 2013). Transit surveys face similar difficulties, with low luminosities meaning only a small population of M-dwarfs have been photometrically monitored for transits compared with FGK stars. Small telescope surveys such as WASP or HATNet do not detect very faint or red objects and so do not have the ability to cover a significant population of M-dwarfs. Surveys using larger telescopes but single-star monitoring, such as MEarth, do not monitor enough M-dwarfs to probe the frequency of hot Jupiters (Berta, Irwin & Charbonneau 2013). Kepler, with a 1 m aperture, was able to monitor M-dwarfs in its field of view, but since it only covered 100 deg^2, that population has been limited to approximately 4000 M-dwarfs (Dressing & Charbonneau 2013). NGTS is therefore currently the best placed survey to determine the frequency of hot Jupiters orbiting early M-dwarfs, monitoring approximately 20 000 early-type M-dwarfs per year as part of the regular search campaigns. However, robust statistics will only be available after a larger number of fields (hence M-dwarfs) have been monitored over the coming years.

4.2 *JWST* potential

The suite of instruments on-board the *JWST* will allow for detailed characterization of transiting exoplanets (Beichman et al. 2014). In particular, transmission spectroscopy of short-period transiting gas giant planets is foreseen as one of the key tasks early in the mission lifetime (Stevenson et al. 2016).

At $J = 12.7$, NGTS-1 is about 2 mag fainter than the 'community targets' proposed by Stevenson et al. (2016) for a *JWST* Early Release Science Program. However, due to the large radius of the planet compared with its host star, the expected transmission signal is relatively high. The signal size per scaleheight, ΔD, assuming a cloud-free atmosphere at a constant equilibrium temperature, T_{eq},

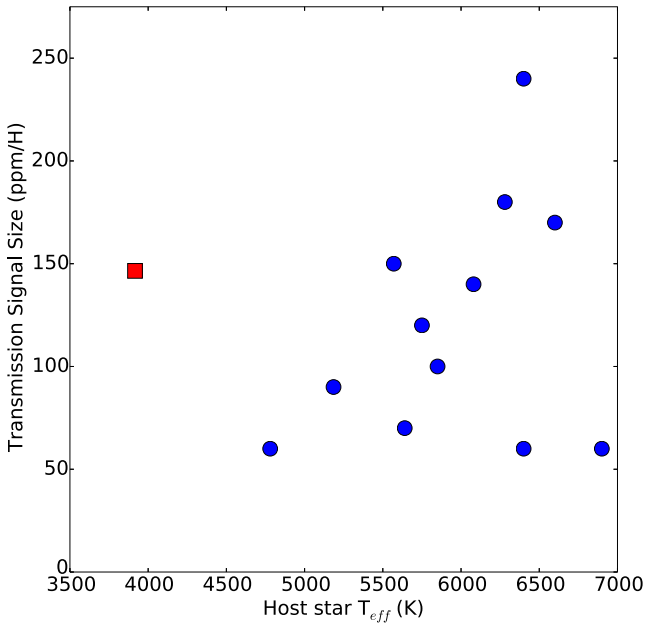

Figure 7. Signal size per scaleheight (in ppm/H) as a function of host star effective temperature for the *JWST* community targets (blue circles; Stevenson et al. (2016)) and NGTS-1b (red square). The signal size for NGTS-1b is comparable to that of the community targets, and it probes planet characterization around a much cooler star than any of the community targets. We note NGTS-1 is fainter by 2 mag than the community targets.

is given by:

$$\Delta D \approx \frac{2k_{\rm B}T_{\rm eq}R_{\rm P}}{\mu g R_{\rm S}^2} \quad (1)$$

where $R_{\rm P}$ and $R_{\rm S}$ are the planetary and stellar radii, respectively, μ is the mean molecular weight, g is the planet's gravity and $k_{\rm B}$ is the Boltzmann constant. Assuming a mean molecular weight of 2.2 u, and applying a factor of 0.5 to account for the transit being grazing, we calculate a signal size of $\Delta D = 146$ for NGTS-1b. We see NGTS-1b has a signal comparable to the *JWST* community targets, though with a very different host star mass (see Fig. 7). In addition, the short period of NGTS-1b ($P = 2.647\,298 \pm 0.000\,020$ d) means there will be many available transits per year, and its location on the sky ($05^{\rm h}30^{\rm m}51\overset{\rm s}{.}45$, $-36^{\circ}37'50\overset{''}{.}83$) means that it lies $\approx 30^{\circ}$ from the *JWST* southern continuous viewing zone, which will allow for over 200 d per year of observing opportunity from *JWST*. The complicating factor here is the fact that NGTS-1b is undergoing a grazing transit, which means that robust atmospheric transmission spectroscopy will require a better understanding of the limb darkening parameters for this host star than is typically the case for a more centrally crossing transit. It also means the transit is shorter in duration, so there is less in-transit time per orbit for transmission spectroscopy.

4.3 Possible thick disc membership

As discussed in Section 3.5, the kinematics of NGTS-1 is consistent with a star from the thick disc population. Additionally, this M-dwarf appears to be slowly rotating and shows no signs of activity from both photometric and spectroscopic indicators. Therefore it seems likely that this system is very old, indicating that giant planet formation around M-dwarfs was possible from an early point in the Galaxy's history. However IR spectroscopy will help determine if the stellar metallicity confirms this picture, as will the more robust distance measurement which will be part of *Gaia* DR2.

5 CONCLUSIONS

The discovery of NGTS-1b demonstrates the capability of NGTS to probe early M-dwarfs for transiting planets – the result of the 20-cm aperture telescopes coupled to red-sensitive CCDs. In the full course of the survey, enough early M-dwarfs will be monitored to allow us to provide statistics for these host stars such as the frequency of hot Jupiters around early M-dwarfs.

The *TESS* mission (Ricker et al. 2014) plans to focus on early M-dwarfs in order to be able to detect potentially habitable planets. NGTS-1 has an *i*-band magnitude of 14.38 ± 0.02, which for *TESS* will be in a sky- and readout-limited regime and therefore will only have an expected precision of 3 mmag per hour (cf. the NGTS light curve is much *better* than this expected *TESS* precision at this magnitude). However, given the depth of the NGTS-1b transit and the approximately continuous observing window function from *TESS*, planets similar to NGTS-1b should be picked up very easily by *TESS* promising to shed more light on giant planets around low-mass stars.

ACKNOWLEDGEMENTS

Based on data collected under the NGTS project at the ESO La Silla Paranal Observatory. The NGTS facility is operated by the consortium institutes with support from the UK Science and Technology Facilities Council (STFC) project ST/M001962/1.

Contributions at the University of Geneva by DB, FB, BC, LM and SU were carried out within the framework of the National Centre for Competence in Research 'PlanetS' supported by the Swiss National Science Foundation (SNSF). The contributions at the University of Warwick by PJW, RGW, DLP, FF, DA, BTG and TL have been supported by STFC through consolidated grants ST/L000733/1 and ST/P000495/1. The contributions at the University of Leicester by MGW and MRB have been supported by STFC through consolidated grant ST/N000757/1.

CAW acknowledges support from the STFC grant ST/P000312/1. TL was also supported by STFC studentship 1226157. MNG is supported by the STFC award reference 1490409 as well as the Isaac Newton Studentship. JSJ acknowledges support by Fondecyt grant 1161218 and partial support by CATA-Basal (PB06, CONICYT). This project has received funding from the European Research Council (ERC) under the European Union's Horizon 2020 research and innovation programme (grant agreement No 681601). The research leading to these results has received funding from the European Research Council under the European Union's Seventh Framework Programme (FP/2007-2013)/ERC Grant Agreement n. 320964 (WDTracer). We thank Andy Read (University of Leicester) for useful discussions on the XMM-Slew Survey data.

REFERENCES

Akeson R. L. et al., 2013, PASP, 125, 989

Allard F., Homeier D., Freytag B., 2011, in Johns-Krull C., Browning M. K., West A. A., eds, ASP Conf. Ser. Vol. 448. 16th Cambridge Workshop on Cool Stars, Stellar Systems, and the Sun. Astron. Soc. Pac., San Francisco, p. 91

Andrews S. M., Rosenfeld K. A., Kraus A. L., Wilner D. J., 2013, ApJ, 771, 129

Anglada-Escudé G. et al., 2016, Nature, 536, 437

Astudillo-Defru N. et al., 2017, A&A, 602, A88
Beichman C. et al., 2014, PASP, 126, 1134
Benedict G. F. et al., 2016, AJ, 152, 141 (B16)
Berdiñas Z. M., 2016, PhD thesis, Instituto de Astrofísica de Andalucía-CSIC; Universidad de Granada, doi:10.5281/zenodo.438330
Berta Z. K., Irwin J., Charbonneau D., 2013, ApJ, 775, 91
Berta-Thompson Z. K. et al., 2015, Nature, 527, 204
Bertin E., Arnouts S., 1996, A&AS, 117, 393
Bonfils X. et al., 2005, A&A, 443, L15
Bonfils X. et al., 2013, A&A, 549, A109
Buchhave L. A., Latham D. W., 2015, ApJ, 808, 187
Charbonneau D. et al., 2009, Nature, 462, 891
Chazelas B. et al., 2012, Proc. SPIE, 8444, 84440E
David T. J. et al., 2016, Nature, 534, 658
Demory B.-O., Seager S., 2011, ApJS, 197, 12
Dressing C. D., Charbonneau D., 2013, ApJ, 767, 95
Fischer D. A., Valenti J., 2005, ApJ, 622, 1102
Fressin F. et al., 2013, ApJ, 766, 81
Gaia Collaboration et al., 2016, A&A, 595, A2
Gillen E., Hillenbrand L. A., David T. J., Aigrain S., Rebull L., Stauffer J., Cody A. M., Queloz D., 2017, ApJ, 849, 11
Gillon M. et al., 2017, Nature, 542, 456
Günther M. N., Queloz D., Demory B.-O., Bouchy F., 2017a, MNRAS, 465, 3379
Günther M. N. et al., 2017b, MNRAS, 472, 295
Hartman J. D. et al., 2015, AJ, 149, 166
Hatzes A. P., Rauer H., 2015, ApJ, 810, L25
Henden A., Munari U., 2014, Contr. Astron. Obser. Skalnate Pleso, 43, 518
Henry T. J., Jao W.-C., Subasavage J. P., Beaulieu T. D., Ianna P. A., Costa E., Méndez R. A., 2006, AJ, 132, 2360
Jenkins J. S. et al., 2017, MNRAS, 466, 443
Johnson J. A. et al., 2012, AJ, 143, 111
Kennedy G. M., Kenyon S. J., 2008, ApJ, 673, 502
Kovács G., Zucker S., Mazeh T., 2002, A&A, 391, 369
Laughlin G., Bodenheimer P., Adams F. C., 2004, ApJ, 612, L73
Lépine S., Hilton E. J., Mann A. W., Wilde M., Rojas-Ayala B., Cruz K. L., Gaidos E., 2013, AJ, 145, 102
Lomb N. R., 1976, Ap&SS, 39, 447
McCormac J. et al., 2017, PASP, 129, 025002
McQuillan A., Aigrain S., Mazeh T., 2013, MNRAS, 432, 1203
Mann A. W., Feiden G. A., Gaidos E., Boyajian T., von Braun K., 2015, ApJ, 804, 64 (M15)
Mayor M. et al., 2003, The Messenger, 114, 20
Meyer M. R., Amara A., Reggiani M., Quanz S. P., 2017, preprint (arXiv:1707.05256)
Nutzman P., Charbonneau D., 2008, PASP, 120, 317
Pepper J. et al., 2017, AJ, 153, 177
Rebassa-Mansergas A., Gänsicke B. T., Rodríguez-Gil P., Schreiber M. R., Koester D., 2007, MNRAS, 382, 1377
Ricker G. R. et al., 2014, Proc. SPIE, 9143, 914320
Roberts D. H., Lehar J., Dreher J. W., 1987, AJ, 93, 968
Robin A. C., Reylé C., Derrière S., Picaud S., 2003, A&A, 409, 523
Rojas-Ayala B., Covey K. R., Muirhead P. S., Lloyd J. P., 2010, ApJ, 720, L113
Rowe J. F. et al., 2014, ApJ, 784, 45
Savcheva A. S., West A. A., Bochanski J. J., 2014, ApJ, 794, 145
Saxton R. D., Read A. M., Esquej P., Freyberg M. J., Altieri B., Bermejo D., 2008, A&A, 480, 611
Skrutskie M. F. et al., 2006, AJ, 131, 1163
Sousa S. G. et al., 2008, A&A, 487, 373
Stelzer B., Marino A., Micela G., López-Santiago J., Liefke C., 2013, MNRAS, 431, 2063
Stevenson K. B. et al., 2016, PASP, 128, 094401
Tamuz O., Mazeh T., Zucker S., 2005, MNRAS, 356, 1466
Triaud A. H. M. J. et al., 2013, A&A, 551, A80
Wheatley P. e. a., 2017, MNRAS, preprint (arXiv:1710.11100),
Wheatley P. J. et al., 2013, Eur. Phys. J. Web Conf. EDP Sciences, p. 13002
Wright E. L. et al., 2010, AJ, 140, 1868
Zacharias N., Finch C. T., Girard T. M., Henden A., Bartlett J. L., Monet D. G., Zacharias M. I., 2013, AJ, 145, 44

SUPPORTING INFORMATION

Supplementary data are available at *MNRAS* online.

Table 1. NGTS photometry for NGTS-1.
Table 2. z-band Eulercam photometry for NGTS-1.

Please note: Oxford University Press is not responsible for the content or functionality of any supporting materials supplied by the authors. Any queries (other than missing material) should be directed to the corresponding author for the article.

[1]*Observatoire de Genève, Université de Genève, 51 Ch. des Maillettes, CH-1290 Sauverny, Switzerland*
[2]*Astrophysics Group, Cavendish Laboratory, J.J. Thomson Avenue, Cambridge CB3 0HE, UK*
[3]*Institute of Planetary Research, German Aerospace Center, Rutherford-strasse 2, D-12489 Berlin, Germany*
[4]*Department of Physics, University of Warwick, Gibbet Hill Road, Coventry CV4 7AL, UK*
[5]*Centre for Exoplanets and Habitability, University of Warwick, Gibbet Hill Road, Coventry CV4 7AL, UK*
[6]*Department of Physics and Astronomy, Leicester Institute of Space and Earth Observation, University of Leicester LE1 7RH, UK*
[7]*Astrophysics Research Centre, School of Mathematics and Physics, Queen's University Belfast, BT7 1NN Belfast, UK*
[8]*Institute of Astronomy, University of Cambridge, Madingley Rise, Cambridge CB3 0HA, UK*
[9]*Departamento de Astronomia, Universidad de Chile, Casilla 36-D, Santiago, Chile*
[10]*Centro de Astrofísica y Tecnologías Afines (CATA), Casilla 36-D, Santiago, Chile*
[11]*Instituto de Astronomia, Universidad Católica del Norte, Casa Central, Angamos 0610, Antofagasta, Chile*
[12]*Center for Astronomy and Astrophysics, TU Berlin, Hardenbergstr. 36, D-10623 Berlin, Germany*

This paper has been typeset from a TEX/LATEX file prepared by the author.